Soft Matter

www.rsc.org/softmatter

Volume 9 | Number 48 | 28 December 2013 | Pages 11429–11720

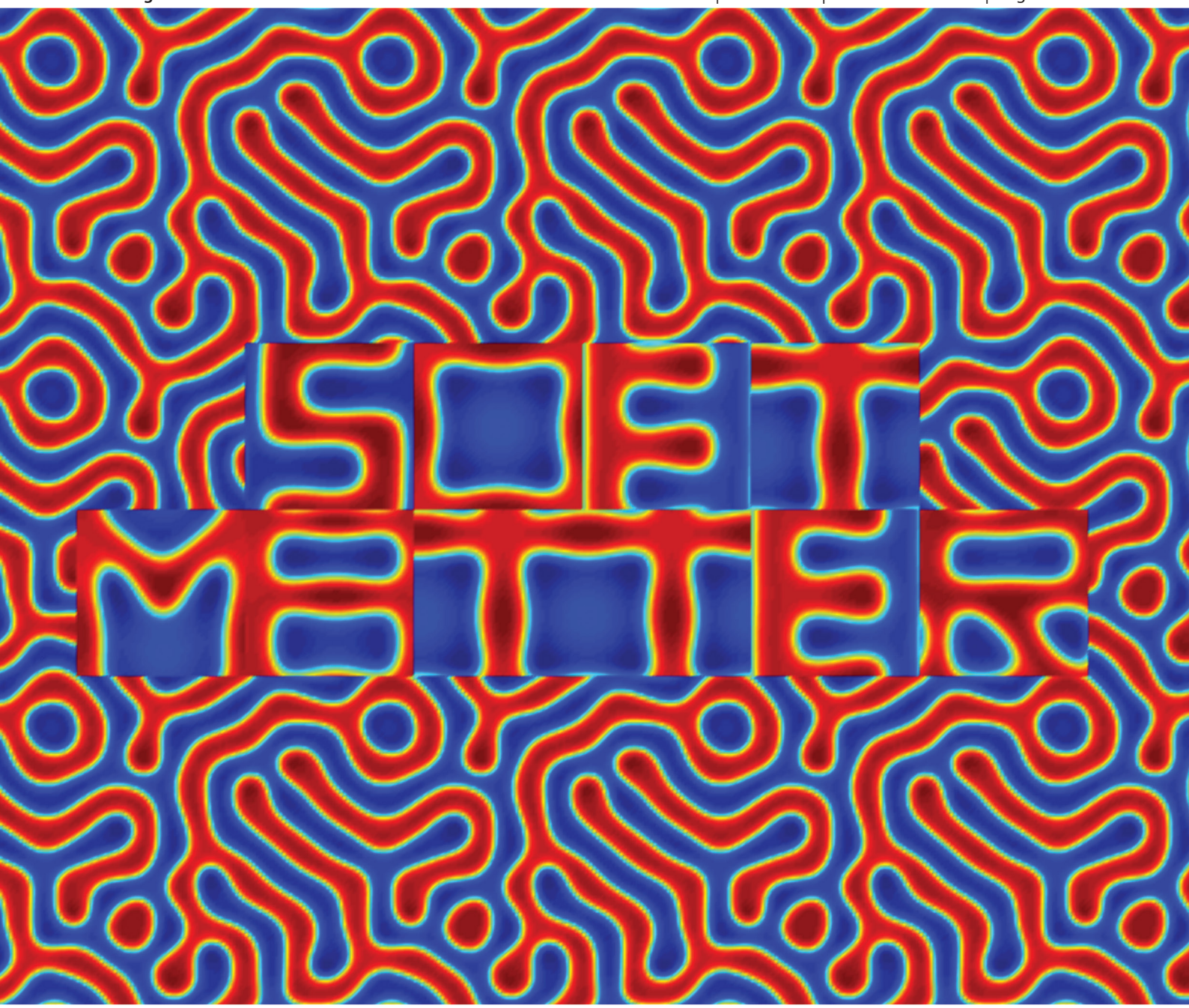

ISSN 1744-683X

RSC Publishing

PAPER

Juan J. de Pablo *et al.*

Evolutionary pattern design for copolymer directed self-assembly

Soft Matter

RSC Publishing

PAPER

View Article Online
View Journal | View Issue

Cite this: *Soft Matter*, 2013, **9**, 11467

Evolutionary pattern design for copolymer directed self-assembly

Jian Qin,[a] Gurdaman S. Khaira,[a] Yongrui Su,[a] Grant P. Garner,[a] Marc Miskin,[b] Heinrich M. Jaeger[b] and Juan J. de Pablo*[ac]

Received 19th July 2013
Accepted 9th October 2013

DOI: 10.1039/c3sm51971f

www.rsc.org/softmatter

Directed assembly of block polymers is rapidly becoming a viable strategy for lithographic patterning of nanoscopic features. One of the key attributes of directed assembly is that an underlying chemical or topographic substrate pattern used to direct assembly need not exhibit a direct correspondence with the sought after block polymer morphology, and past work has largely relied on trial-and-error approaches to design appropriate patterns. In this work, a computational evolutionary strategy is proposed to solve this optimization problem. By combining the Cahn–Hilliard equation, which is used to find the equilibrium morphology, and the covariance-matrix evolutionary strategy, which is used to optimize the combined outcome of particular substrate–copolymer combinations, we arrive at an efficient method for design of substrates leading to non-trivial, desirable outcomes.

1 Introduction

Lithography represents one of the key fabrication steps for nanoscopic devices, ranging from electronic circuits to storage media.[1] As critical device dimensions continue to shrink, alternative patterning strategies and materials are being sought to circumvent some of the challenges that arise at small length scales. These include roughness, pattern collapse, and defectivity. In recent years, the directed assembly of block copolymers on topographic or chemical patterns has received considerable attention as a viable and promising approach for lithographic patterning of ultra-small features. Block copolymers are known to spontaneously self-assemble into a wide range of ordered morphologies, including lamellar, cylindrical, and spherical structures.[1,2] In thin films, the self-assembly can be directed through the use of chemical or topographic patterns on the underlying substrate. The basic elements of "directed self-assembly" are described schematically in Fig. 1, where one can appreciate some of its main attributes, as well as some of the challenges that may arise. Past work has shown that it is possible to guide the assembly of simple diblock copolymers and their blends with homopolymers into all of the canonical features that arise in integrated circuits, including lines, bends, jogs, and spots.[2] An important concept in directed self-assembly is pattern interpolation, in which only a subset of any desirable features appears on the substrate, and the block copolymer is used to fill-in the rest, thereby adding information to the fabrication process. For example, as illustrated in Fig. 1, to produce a dense array of cylinders, one only needs to use a surface pattern that includes a fraction of the cylinders (*e.g.* one-fourth). Such patterns then serve as a guiding template for a cylinder forming diblock copolymer having a period that is two times smaller than the period of the surface spots.

Dense, periodic arrays of lines or spots are of considerable interest for applications in dense storage media.[3–8] As explained in Fig. 1 in the context of so-called "bit-patterned media", in order to produce next-generation hard drives it is of interest to pattern isolated "bits" that would subsequently be filled with magnetic material. Current efforts seek to produce such bits with a pitch in the vicinity of 10 nm, which would result in storage densities that are well above those available today. As shown by Ruiz *et al.*,[3] the underlying pattern used to direct the assembly of a cylinder forming diblock copolymer need not

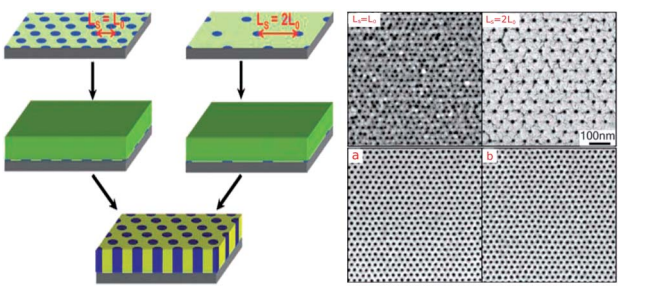

Fig. 1 Left: schematic illustration showing self-assembly on a patterned substrate with pattern rectification and density multiplication. Right: experimental results[3] on PS-PMMA diblocks showing the effects of directed self-assembly. Block copolymer's natural periodicity: $L_0 = 27$ nm.

[a]*Institute for Molecular Engineering, University of Chicago, Chicago, IL 60637, USA. E-mail: depablo@uchicago.edu*

[b]*James Franck Institute and Department of Physics, University of Chicago, Chicago, IL 60637, USA*

[c]*Institute for Molecular Engineering, Argonne National Laboratory, Argonne, IL 70439, USA*

have the same density as the final storage device; one can pattern a subset of spots on the substrate, and then use the copolymer to create additional bits, thereby doubling, quadrupling, or generally multiplying the storage density of a device. For more complex layouts, such as those encountered in logic devices, a central challenge is to guide the materials to assemble into aperiodic, more versatile, and more complicated morphologies or geometries. Within the spirit of density multiplication, the underlying pattern used to guide the assembly need not have a one-to-one correspondence with the geometry of interest; the question that arises then is, for a target morphology, how can one design an optimal sparse pattern to direct block copolymer self-assembly?

One could in principle adopt a traditional inverse Monte Carlo algorithm, and rely on a random search of suitable patterns to find a plausible solution. This amounts to a computational trial-and-error search akin to that performed in experiments. Such an approach has been proposed recently[9] with good results in the context of topographically directed assembly. In that work, a simple mean-field theory in two dimensions (SCFT)[10] was combined with a random search algorithm to identify topographic features leading to suitable morphologies. The disadvantage of such an approach is that the search is blind and, for large parameter spaces, it can rapidly become intractable.

In this work, we propose to use a state-of-the-art optimization technique, namely the covariance-matrix adaptation evolutionary strategy (CMA-ES),[11] in combination with a mean field copolymer model, to identify optimal chemical patterns for assembly of block polymers into non-regular morphologies.

2 Methodology

For concreteness, the strategy presented in this work is described in the context of a surface pattern consisting of circular spots. Extensions to other types of patterns are trivial. The goal is to use the minimal number of spots on the surface to direct the assembly of a lamellae-forming diblock copolymer into a target morphology. To determine the equilibrium copolymer morphology for a given placement of the surface spots, we use the Ginzburg–Landau (GL) free energy functional, and we evolve the morphology using the Cahn–Hilliard (CH) equation.[12] One could use other approaches, including more elaborate mean field theories, theoretically informed approaches, or full-blown molecular simulations, but a generic GL–CH approach is simple and allows us to demonstrate the general principles put forth in this work without loss of generality. Furthermore, it facilitates studies of large systems, and enables simulations of the evolution dynamics of any given morphology.[13,14]

In order to evolve a particular combination of spots and morphology in parameter space, we introduce an objective or "fitness" function that quantifies the difference between the target morphology and the equilibrium morphology corresponding to certain pole positions. That function depends on the spot positions, with the number of spots held constant. The fitness function is then minimized with a covariance matrix adaptation evolutionary strategy (CMA-ES).[11] CMA-ES is based on the idea of "natural selection", and has proven to be particularly efficient for optimization of complicated functions when little is known about the underlying landscape.[11]

2.1 Cahn–Hilliard equation for assembled morphology

For simplicity, we consider a system of pure diblock copolymers composed of A and B blocks. A and B type monomers have the same reference volume and statistical segment length. The total number of beads and the volume fraction of A blocks are denoted as N and f, respectively. The excess free energy cost of creating an A/B contact is quantified by the Flory–Huggins parameter χ. The product χN controls the degree of phase separation; the higher its value, the stronger the tendency of A and B blocks to segregate.

Following Shi *et al.*,[15,16] we use the free energy form developed by Ohta and Kawasaki[17] to characterize the system morphology. This formalism is valid in the strong segregation regime (large χN); it is expressed as the sum of three terms

$$F[\phi] = F_{\mathrm{GL}}[\phi] + F_{\text{non-local}}[\phi] + \int \mathrm{d}\mathbf{r} H_{\mathrm{ext}}(\mathbf{r})\phi(\mathbf{r}). \quad (1)$$

Here $\phi(\mathbf{r})$ is the order parameter field quantifying the extent of phase separation, defined as the monomer volume fraction difference, $\phi(\mathbf{r}) \equiv \phi_{\mathrm{A}}(\mathbf{r}) - \phi_{\mathrm{B}}(\mathbf{r})$. $H_{\mathrm{ext}}(\mathbf{r})$ is the external potential representing the interaction between the guiding spots and the copolymer; we use the hyperbolic tangent function introduced in ref. 15, $H_{\mathrm{ext}}(\mathbf{r}) = -(1/2)V_0(\tanh(-|\mathbf{r}-\mathbf{R}|+\sigma)/\lambda + 1)$, where $\mathbf{R}$ is the position of the spot center, V_0 is the strength of the potential, σ is the range of the potential, and λ controls the steepness of the decay.

The Ginzburg–Landau free energy $F_{\mathrm{GL}}[\phi]$ can be written as

$$F_{\mathrm{GL}}[\phi] = \int \mathrm{d}\mathbf{r}\left[\frac{1}{2}(\nabla\phi)^2 + W(\phi)\right]. \quad (2)$$

The gradient term represents the free energy cost associated with spatial inhomogeneities. The $W(\phi)$ term is the local free energy density that drives the phase separation. It depends on the Flory–Huggins χ-parameter, and contains only even powers

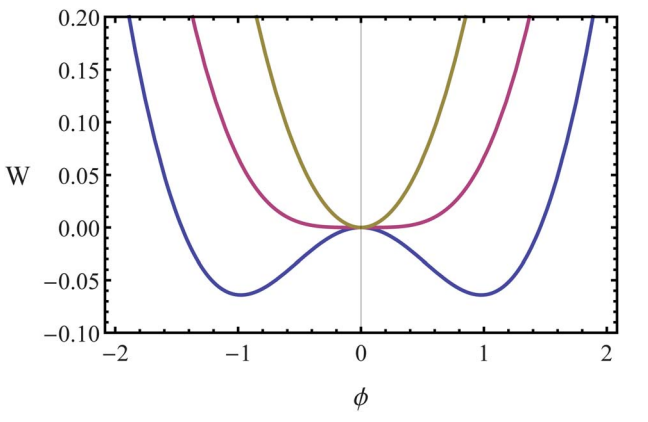

Fig. 2 Local demixing free energy as a function of order parameter. Yellow: $A = 0.5$; red: $A = 1.0$; blue: $A = 1.3$.

of ϕ (this is true since exchanging A and B block labels has no physical consequence). W is generally assumed to be of the form $(1/2)\phi^2 + (g/4)\phi^4$. In this work, following Shi *et al.*,[15] we set $W = -A \ln\cosh(\phi) + \phi^2/2$. Here the parameter A controls the degree of phase separation. W has one minimum at $\phi = 0$ for $A < 1$ and has two minima for $A > 1$. The shapes of W at $A = 0.5$, 1.0, and 1.3 are shown in Fig. 2.

The term $F_{\text{non-local}}$ is the chain stretching energy describing the chain connectivity. It can be written as[15,17]

$$F_{\text{non-local}} = \frac{\alpha}{2}\int d\mathbf{r}\int d\mathbf{r}'\delta\phi(\mathbf{r})G(\mathbf{r}-\mathbf{r}')\delta\phi(\mathbf{r}'), \quad (3)$$

where $\delta\phi(\mathbf{r}) \equiv \phi(\mathbf{r}) - \bar{\phi}$ is the deviation from the homogeneous value, and $\bar{\phi} = 2f - 1$. $G(\mathbf{r},\mathbf{r}')$ satisfies $-\nabla^2 G(\mathbf{r},\mathbf{r}') = \delta(\mathbf{r}-\mathbf{r}')$. For simplicity, we consider a two-dimensional representation here, where $G(\mathbf{r},\mathbf{r}') = -\ln(|\mathbf{r}-\mathbf{r}'|)/2\pi$.[17]

Eqn (2) and (3) are purely phenomenological. The mean field free energy for a diblock copolymer melt may be mapped onto this form by using the explicit expressions in ref. 17 (eqn. (4.5)–(7)). By inspection, one can arrive at the following mapping rules: first, the length scales in eqn (2) and (3) are in units of ξ_0, where ${\xi_0}^2$ is defined by ${R_g}^2/(4f(1-f)\chi_s N)$ and R_g is the radius of gyration of the diblock copolymer; second, the value of A equals χ/χ_s, where χ_s is the value of the mean field spinodal ($\chi_s = 10.5/N$ for $f = 0$); third, the value of α equals $3/(16f^3(1-f)^3(\chi_s N)^2)$. The extent of the phase separation is controlled by the value of χ or A. The equilibrium domain spacing is proportional to $N^{2/3}(A-1)^{1/6}$.[17]

To find the equilibrium morphology, we use the Cahn–Hilliard equation to evolve the ϕ field, which is appropriate for conserved order parameters and has been widely used to study the material structural evolution in phase field models.[18] The Cahn–Hilliard equation has the form

$$\frac{\partial\phi(\mathbf{r},t)}{\partial t} = M\nabla^2\frac{\delta F[\phi]}{\delta\phi(\mathbf{r},t)}, \quad (4)$$

where M is the effective mobility coefficient and is set to unity. Substituting the free energy expression in the Cahn–Hilliard equation, we get[15]

$$\frac{\partial\phi(\mathbf{r},t)}{\partial t} = \nabla^2\big(-\nabla^2\phi(\mathbf{r},t) - A\tanh(\phi(\mathbf{r},t)) + \phi(\mathbf{r},t)\big) + \nabla^2 H_{\text{ext}}(\mathbf{r}) - \alpha\delta\phi(\mathbf{r},t). \quad (5)$$

Since the Cahn–Hilliard equation is essentially a diffusion equation, the total monomer content in the system remains constant as time evolves, *i.e.*, $\int d\mathbf{r}\phi(\mathbf{r},t) = \bar{\phi}V$, where V is the volume of the system. For a given block volume fraction f and given spot positions, the values of A, α, and $H_{\text{ext}}(\mathbf{r})$ are fixed. The effect of f is implicit in the $\delta\phi$ term. For random initial field values satisfying the stoichiometric constraint, after a sufficiently long time, the Cahn–Hilliard equation will typically evolve the system into a local equilibrium state.

2.2 CMA-ES optimization

The target morphology is described by $\tilde{\phi}(\mathbf{r})$, and the equilibrium morphology under a given set of spot constraints by $\phi(\mathbf{r};\{\mathbf{R}_i\})$, where the dependence on pole position vectors $\{\mathbf{R}_i\}$ is explicitly shown. The difference between ϕ and $\tilde{\phi}$ can be quantified by

$$\Omega(\{\mathbf{R}_i\}) \equiv \int d\mathbf{r}(\phi(\mathbf{r};\{\mathbf{R}_i\}) - \tilde{\phi}(\mathbf{r}))^2. \quad (6)$$

Our first goal is to optimize spot positions by minimizing Ω.

We resort to the covariance matrix adaptation evolutionary strategy or CMA-ES to minimize Ω. CMA-ES belongs to a family of evolutionary optimization algorithms that mimic some of the principles of biological evolution.[11] Recently, it has been used with considerable success in the context of materials research for optimization of packing problems[19] and for crystal structure prediction[20] (the use of different variants of evolutionary algorithms has also been reported[21,22]). It is iterative, stochastic, and does not require that the derivative of the objective function be evaluated. At each iteration stage or generation, a finite number (λ) of samples derived from the previous generation is allowed to mutate and recombine following a prescribed protocol; these offspring are then ranked according to the objective function, and the "best" μ offsprings are used for the iteration of the next generation.

The key to implementing such an algorithm is designing an efficient protocol for mutation and recombination, which on the one hand maintains the population diversity, so that the system is not trapped into local extrema, and on the other hand ensures fast convergence in the neighborhood of the optimal extremum. In a naive random search, the older population is perturbed by independently distributed Gaussian random numbers. In CMA-ES, however, the correlation among different searching directions, as measured by the covariance matrix, is explicitly considered, and the covariance matrix is adapted at each iteration step by "learning" from the fitness of the entire population. The idea is analogous to the approximation of the Hessian matrix in the quasi-Newton method in deterministic optimization.

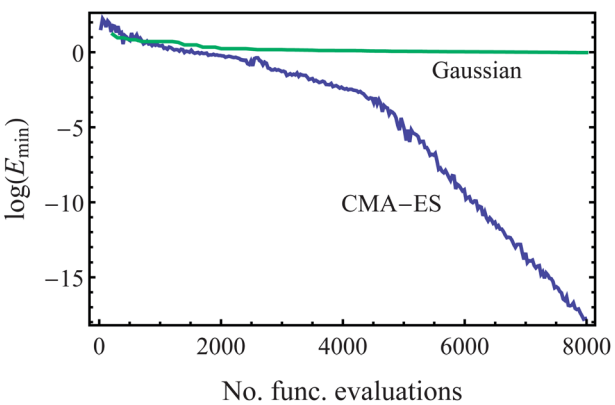

Fig. 3 Convergence behavior of CMA-ES compared to a Gaussian random search, tested on the 12-dimensional Rosenbrock function, which has a global minimum at zero when all its arguments equal unity. The range for the Gaussian random search is varied using the "1/5" acceptance rate rule.[11] The CMA-ES uses an evolution population of 28 members, out of which 4 best members are selected at each generation. In both cases, the initial point is generated at random.

Our implementation of the CMA-ES is based on the improved algorithm discussed in ref. 23. Most parameters required by the algorithm have been set on the basis of heuristic arguments. For our problem, the population size λ and the number of offsprings used to generate new populations μ are 28 and 4, respectively (the ratio of the two was recommended to be 7; see ref. 23). Note that the size of the population ultimately determines the quality of the solution; for the systems considered here, we do not see significant improvements when the population and offspring numbers are increased beyond 28 and 4, respectively. To examine the convergence behavior of CMA-ES, in Fig. 3, we compared the optimization results obtained from CMA-ES and the Gaussian random search for the 12-dimensional Rosenbrock function. Although the exact shape of the convergence curve depends slightly on the location of the starting point, the curves in the figure are representative of the typical efficiency of both methods. It is apparent that the Gaussian random search is frequently trapped in local minima, whereas the CMA-ES is able to find the global minimum. Furthermore, the convergence rate is exponential after a sufficient number of iterations.

3 Results

For the problem of interest here, solving the CH equation is the most computationally demanding step. With that issue in mind, in Section 3.1 we focus on the algorithm and optimize the parameters used to solve the CH equation. Then, in Section 3.3, we present the optimization results obtained using the CMA-ES algorithm.

3.1 Evolving Cahn–Hilliard equation

To solve the CH equation, we discretize the square-shaped simulation cell into an N-by-N grid, and approximate the gradient term in eqn (5) using central differences. The composition field $\phi(\mathbf{r}, t)$ is propagated in time using the forward Euler's method, with δt as the time step (effectively, the mobility factor M can be absorbed into the definition of δt). The algorithm complexity scales with N^2, as confirmed by Fig. 4, in which the time spent on a fixed number of CH equation iterations is plotted *versus* the number of grid points N, on a logarithmic scale. The results can be fit with a straight line of slope 2.

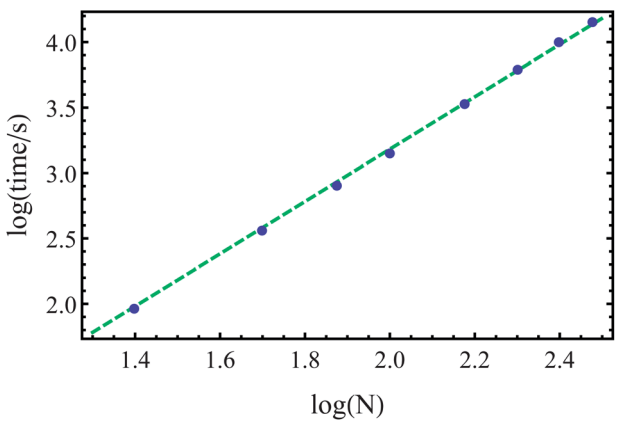

Fig. 4 Numerical complexity of the algorithm for the CH equation. The abscissa corresponds to the number of grid point per edge N. The ordinate axis corresponds to the time spent on 2×10^5 iteration steps. The dashed line has a slope of 2. Parameters: $A = 1.3$, $\alpha = 0.002$, $f = 0.5$, and $\delta t = 0.02$.

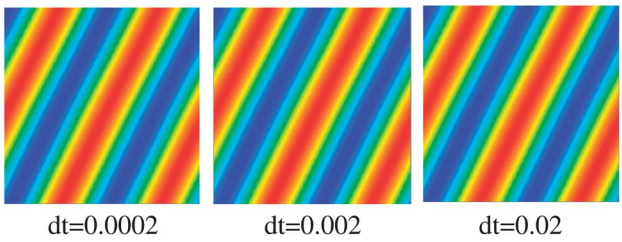

Fig. 5 Effects of δt on equilibrium morphology. Equilibrium morphologies are obtained by propagating the CH equation with three different values of time step: 0.0002, 0.002, and 0.02. Parameters: $A = 1.3$, $\alpha = 0.02$, $N = 50$.

To find a proper value of time step δt that is small enough to ensure numerical stability yet large enough to evolve the CH equation efficiently, we compared results obtained at different δt values. Fig. 5 shows equilibrium morphologies obtained by solving the CH equation using three different values of δt, starting from the same initial configuration and terminating at time $t = 4000$. The fact that the three morphologies are nearly indistinguishable suggests that using $\delta t = 0.02$ is sufficient. In the remainder of this work, we use this value for our calculations.

The other parameter to be optimized is the number of iteration steps. In our study, we want this number to be sufficiently large to allow the system to reach the equilibrium morphology for a given arrangement of the spots; at the same time, we also want to avoid spending efforts on equilibrated morphologies. Fig. 6 shows the morphologies at different times along the same trajectory. It is clear that after at least 10^5 iteration steps, which correspond to $t = 2000$, the equilibrium morphology has been found. For the results presented in the next section, we used an iteration number of 2×10^5, which ensures that the local equilibrium morphology is found for each simulation.

3.2 Phase diagram in the A–f plane

Before optimizing the spot positions using the evolutionary algorithm, we explored the effects of various controlling parameters in the generic CH equation. Fig. 7 shows the typical morphologies obtained for various values of A and f, and at a

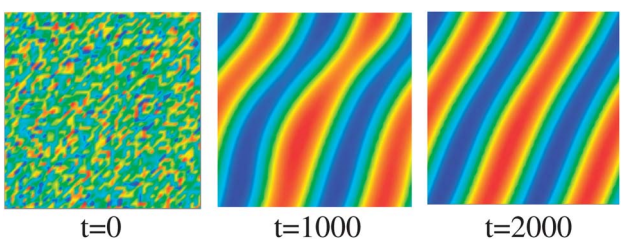

Fig. 6 Time dependence of the morphology evolution. Morphologies at different times along the same evolution trajectory using $\delta t = 0.02$. Parameters: $A = 1.3$, $\alpha = 0.002$, $N = 50$.

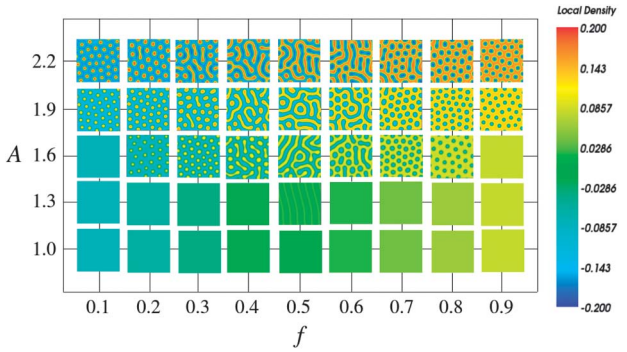

Fig. 7 2-D phase diagram at varying values of A and f, for $\alpha = 0.02$. Morphologies are obtained by evolving the CH equation for 2×10^8 steps from a random initial configuration ($\delta t = 0.01$). The grid size: 100×100.

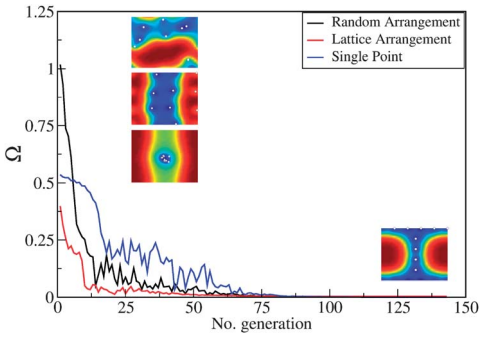

Fig. 9 Convergence behavior of the CMA-ES optimization using three different ways of generating the initial set of pole arrangements: (1) completely random; (2) lattice based; (3) at the same starting point.

fixed value of α. As discussed in Section 2, f is the block volume fraction that controls the symmetry of the morphology, and A is analogous to the χ parameter, which controls the strength of block incompatibility.

The results in Fig. 7 are consistent with the physical meaning of A and α. For $A \leq 1.0$, homogeneous morphologies are found for all f values. For $A > 1.0$, the lamellar patterns are found at compositions close to $f = 0.5$, and the hexagonally packed cylindrical morphologies are found at asymmetric compositions, even though in both cases the presence of defects is apparent.

In what follows, we focus on systems forming a lamellar morphology, and use the following parameters: $A = 1.3, f = 0.5$, and $\alpha = 0.002$. This set of parameter gives distinct lamellae having a natural periodicity of $L_0 \simeq 20$.

3.3 Optimization using evolutionary algorithm

We now present results obtained using the CMA-ES optimization. As mentioned above, the population size is $\lambda = 28$, and the number of fitting samples used to spawn new trajectories is $\mu = 4$. The first target morphology defined here is a pattern mimicking the letter "I", shown in Fig. 8(b). The number of anchoring spots representing the chemical pattern is 9. Initial spot positions are generated at random, and the initial morphology is calculated by evolving the CH equation, as shown in the inset of Fig. 8(a). At each iteration step, the spots are repositioned using the CMA-ES algorithm, and the equilibrium morphology is generated by solving the CH equation. The values of the objective function are calculated using eqn (6) and are plotted in Fig. 8(a), as a function of iteration number (also see the inset for a plot on a logarithmic scale). The results suggest that the magnitude of the objective function decays nearly exponentially, and that there exists two convergence rate regimes. The first (below 150 iterations) has a smaller slope; the second regime (above 150 iterations) has a greater slope. The existence of these two regimes mimics the behavior shown in Fig. 3, implying that the spot positions are first optimized globally, and then locally. The results also show that the optimal spot positions are identified within 250 evolution iterations, and that the residual value of the objective function drops to the level of 10^{-8}. The final configuration and the corresponding spot positions are shown in Fig. 8(c).

To verify that the solution identified by CMA-ES is at least a local optimal, we performed the following test: we first place the spots at ideal positions that are likely to generate the "I" pattern, and then use the solution of the CH equation as the target morphology and re-iterate from a random state. Since now the target morphology is a solution of the CH equation, it is also a well-defined minimum of the objective function eqn (6), and ideally the minimum should be bracketed by the CMA-ES algorithm. This is indeed confirmed by our results. On the other hand, in general, the exact spot positions obtained from CMA-ES optimization depend slightly on the initial configuration. One way to reduce this dependence is to conduct multiple optimizations, and use the average.

To further demonstrate that the CMA-ES only has a weak dependence on the initial pole arrangement, we show in Fig. 9

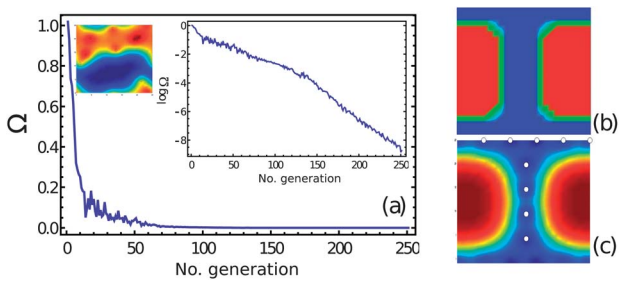

Fig. 8 Evolutionary results of the "I" pattern. (a) Evolution of the objective function; (b) the target morphology. (c) The optimal morphology and the spot positions. Parameters: $A = 1.3$, $\alpha = 0.002$, and $N = 50$.

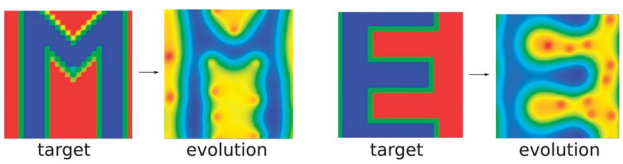

Fig. 10 Target and optimal morphologies for the "M" and "E" patterns. The parameter set is the same as that in Fig. 8.

the optimization results obtained using three distinct ways of generating the initial pole arrangement, by placing poles: (1) randomly, (2) regularly on a lattice, and (3) at a single point. In all three cases, the convergence rates as evidenced by the objective function values are comparable, and the converged morphologies are nearly identical. Indeed, one particularly attractive feature of the CMA-ES optimization is that it has a stronger dependence on the initial step size (searching radius) than the initial pole position. Furthermore, the searching radius in CMA-ES is self-adaptive; the algorithm can refine the value progressively as the morphologies are evolved based on the closeness to the target morphology.

To further test the efficiency of the CMA-ES algorithm, we used several other nontrivial patterns. Two sets of target and optimized morphologies are shown in Fig. 10, which mimic the letters "M" and "E", respectively. Both of these two patterns are generated using the same parameter set as the pattern "I", and the convergence behaviors are similar.

4 Summary

We have presented a methodology to solve the pattern design problem by using a Cahn–Hilliard equation to find the equilibrium morphology of diblock copolymers and by using the CMA-ES algorithm to optimize the underlying chemical pattern. The applicability and usefulness of the proposed strategy were demonstrated by using lamellar forming diblock copolymers to create three nontrivial target morphologies.

The size of the systems considered here was modest, about $2L_0 \times 2L_0$, and the overall calculation time required to generate an optimal solution was approximately 8 hours on a single processor. The extension of the methodology to larger systems and different morphologies is straightforward. The computational efficiency of the proposed approach could be easily increased by using parallel algorithms: (1) as shown in Fig. 4, the numerical complexity for solving the CH equation scales with the system size (N^2). This step involves essentially matrix-vector products, and can be readily parallelized. (2) The CMA-ES essentially involves a set of independent populations, which can also be parallelized in a trivial way.

The objective function used in this work is the simplest that one can think of. More elaborate versions could potentially be used to improve the rate of convergence. For instance, instead of calculating the difference in real space, one may consider the difference in Fourier mode coefficients. Assigning different weights to long and short wavelength modes may lead to a more efficient optimization behavior.

The Cahn–Hilliard equation was used in this work to resolve the composition profile. As a generic framework, the equation also enables us to study assembly dynamics, and can be adapted to study more complex systems, including polymer blends.[16] These possibilities will be addressed in future work.

Acknowledgements

This work is supported by the National Science Foundation through the Chicago MRSEC, DMR-0820054, and by the Semiconductor Research Corporation (SRC). Additional support was provided by the Office of Naval Research through MURI N00014-11-1-0690.

Notes and references

1 Y.-C. Tseng and S. B. Darling, *Polymers*, 2010, **2**, 470–489.
2 M. P. Stoykovich, H. Kang, K. C. Daoulas, G. Liu, C.-C. Liu, J. J. de Pablo, M. Müller and P. F. Nealey, *ACS Nano*, 2007, **1**, 168–175.
3 R. Ruiz, H. Kang, F. A. Detcheverry, E. Dobisz, D. S. Kercher, T. R. Albrecht, J. J. de Pablo and P. F. Nealey, *Science*, 2008, **321**, 936.
4 F. A. Detcheverry, G. Liu, P. F. Nealey and J. J. de Pablo, *Macromolecules*, 2010, **43**, 3446.
5 C.-C. Liu, A. Ramírez-Hernández, E. Han, G. S. W. Craig, Y. Tada, H. Yoshida, H. Kang, S. Ji, P. Gopalan, J. J. de Pablo and P. F. Nealey, *Macromolecules*, 2013, **46**, 1415.
6 J. Y. Cheng, C. A. Ross, V. Z.-H. Chan, E. L. Thomas, R. G. H. Lammertink and G. J. Vancso, *Adv. Mater.*, 2001, **13**, 1174–1178.
7 K. Naito, H. Hieda, M. Sakurai and Y. Kamata, *IEEE Trans. Magn.*, 2002, **38**, 1949–1951.
8 K. W. Guarini, C. T. Black, Y. Zhang, I. V. Babich, E. M. Sikorski and L. M. Gignac, *IEEE Int. Electron Devices Meet., Tech. Dig., 50th*, 2003, **2003**, 541–544.
9 A. F. Hannon, K. W. Gotrik, C. A. Ross and A. Alexander-Katz, *ACS Macro Lett.*, 2013, **2**, 251–255.
10 M. W. Matse, *J. Phys.: Condens. Matter*, 2002, **14**, R21.
11 A. E. Eiben and J. E. Smith, *Introduction to Evolutionary Computing*, Springer, 2003.
12 J. W. Cahn and J. E. Hilliard, *J. Chem. Phys.*, 1958, **28**, 258–267.
13 S. Qi and Z.-G. Wang, *J. Chem. Phys.*, 1999, **111**, 10681–10688.
14 K. Yamada, M. Nonomura and T. Ohta, *Macromolecules*, 2004, **37**, 5762–5777.
15 W. Li, F. Qiu, Y. Yang and A.-C. Shi, *Macromolecules*, 2010, **43**, 1644–1650.
16 N. Xie, W. Li, F. Qiu and A.-C. Shi, *Soft Matter*, 2013, **9**, 536–542.
17 T. Ohta and K. Kawasaki, *Macromolecules*, 1986, **19**, 2621–2632.
18 L.-Q. Chen, *Annu. Rev. Mater. Res.*, 2002, **32**, 113–140.
19 M. Z. Miskin and H. M. Jaeger, *Nat. Mater.*, 2013, **12**, 326–331.
20 A. R. Oganov, A. O. Lyakhov and M. Valle, *Acc. Chem. Res.*, 2010, **44**, 227–237.
21 E. Bianchi, G. Doppelbauer, L. Filion, M. Dijkstra and G. Kahl, *J. Chem. Phys.*, 2012, **134**, 214102.
22 M. Dennison, K. Milinković and M. Dijkstra, *J. Chem. Phys.*, 2012, **137**, 044507.
23 N. Hansen, S. D. Müller and P. Koumoutsakos, *Evol. Comput.*, 2003, **11**, 1–18.

